
3D Indoor Instance Segmentation in an Open-World

**Mohamed El Amine Boudjoghra¹, Salwa K. Al Khatib¹, Jean Lahoud¹,
Hisham Cholakkal¹, Rao Muhammad Anwer^{1,2}, Salman Khan^{1,3}, Fahad Shahbaz Khan^{1,4}**

¹Mohamed Bin Zayed University of Artificial Intelligence (MBZUAI),

²Aalto University, ³Australian National University, ⁴Linköping University

{mohamed.boudjoghra, salwa.khatib, jean.lahoud,
hisham.cholakkal, rao.anwer, salman.khan, fahad.khan}@mbzuai.ac.ae

Abstract

Existing 3D instance segmentation methods typically assume that all semantic classes to be segmented would be available during training and only seen categories are segmented at inference. We argue that such a closed-world assumption is restrictive and explore for the first time 3D indoor instance segmentation in an open-world setting, where the model is allowed to distinguish a set of known classes as well as identify an unknown object as unknown and then later incrementally learning the semantic category of the unknown when the corresponding category labels are available. To this end, we introduce an open-world 3D indoor instance segmentation method, where an auto-labeling scheme is employed to produce pseudo-labels during training and induce separation to separate known and unknown category labels. We further improve the pseudo-labels quality at inference by adjusting the unknown class probability based on the objectness score distribution. We also introduce carefully curated open-world splits leveraging realistic scenarios based on inherent object distribution, region-based indoor scene exploration and randomness aspect of open-world classes. Extensive experiments reveal the efficacy of the proposed contributions leading to promising open-world 3D instance segmentation performance. Code and splits are available at: <https://github.com/aminebdj/3D-OWIS>.

1 Introduction

3D semantic instance segmentation aims at identifying objects in a given 3D scene, represented by a point cloud or mesh, by providing object instance-level categorization and semantic labels. The ability to segment objects in the 3D domain has numerous vision applications, including robotics, augmented reality, and autonomous driving. Following the developments in the sensors that acquire depth information, a variety of datasets has been presented in the literature which provides instance-level annotations. In view of the availability of large-scale 3D datasets and the advances in deep learning methods, various 3D instance segmentation methods have been proposed in recent years.

The dependence of 3D instance segmentation methods on available datasets has a major drawback: a fixed set of object labels (vocabulary) is learned. However, object classes in the real world are plentiful, and many unseen/unknown classes can be present at inference. Current methods that learn on a fixed set not only discard the unknown classes but also supervise them to be labeled as background. This prevents intelligent recognition systems from identifying unknown or novel objects that are not part of the background. Given the importance of identifying unknown objects, recent works have explored open-world learning setting for 2D object detection [18, 11, 28, 33]. In the open-world setting, a model is expected to identify unknown objects, and once new classes are labeled, the new set is desired to be incrementally learned without retraining [18]. While previous methods have been mostly suggested for open-world 2D object detection, it is yet to be explored

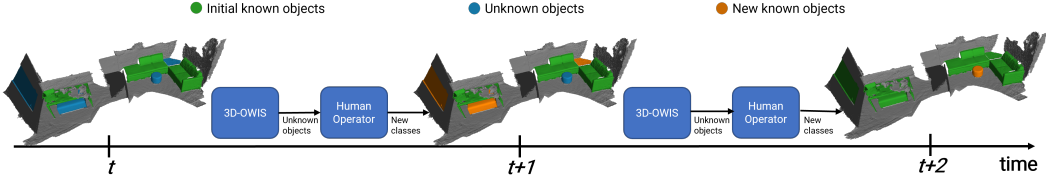


Figure 1: **3D instance segmentation in an open-world.** During each iterative learning phase, the model detects *unknown* objects, and a human operator gradually assigns labels to some of them and incorporates them into the pre-existing knowledge base for further training.

in the 3D domain. The main challenge lies in understanding how objects appear in 3D in order to separate them from the background and other object categories.

3D instance segmentation in the open world, illustrated in Fig. 1, offers more flexibility, allowing the model to identify unknown objects and request annotations for these novel classes from an oracle for further training. However, this approach presents several challenges: (i) the lack of annotations for unknown classes, necessitating quality pseudo-labeling techniques; (ii) the similarities between predicted features of known and unknown classes, requiring separation techniques for improved prediction; and (iii) the need for a more reliable objectness scoring method to differentiate between good and bad predicted masks for 3D point clouds.

In this work, we investigate a novel problem setting, namely open-World indoor 3D Instance Segmentation, which aims at segmenting objects of unknown classes while incrementally adding new classes. We define real-world protocols and splits to test the ability of 3D instance segmentation methods to identify unknown objects. In the proposed setup, unknown object labels are also added incrementally to the set of known classes, akin to real-world incremental learning scenarios. We propose an unknown object identifier with a probability correction scheme that enables improved recognition of objects. To the best of our knowledge, we are the first to explore 3D instance segmentation in an open-world setting. The key contributions of our work are:

- We propose the first open-world 3D indoor instance segmentation method with a dedicated mechanism for accurate identification of 3D unknown objects. We employ an auto-labeling scheme to generate pseudo-labels during training and induce separation in the query embedding space to delineate known and unknown class labels. At inference, we further improve the quality of pseudo-labels by adjusting the probability of unknown classes based on the distribution of the objectness scores.
- We introduce carefully curated open-world splits, having known vs. unknown and then incremental learning over the span of 200 classes, for a rigorous evaluation of open-world 3D indoor segmentation. Our proposed splits leverage different realistic scenarios such as inherent distribution (frequency-based) of object classes, various class types encountered during the exploration of indoor areas (region-based), and the randomness aspect of object classes in the open-world. Extensive experiments reveal the merits of the proposed contributions towards bridging the performance gap between our method and oracle.

2 Related Work

3D semantic instance segmentation: The segmentation of instances in 3D scenes has been approached from various angles. Grouping-based or clustering-based techniques use a bottom-up pipeline by learning an embedding in the latent space to help cluster the object points. [4, 13, 14, 17, 20, 21, 34, 38]. Proposal-based methods work in a top-down fashion, first detecting 3D bounding boxes, then segmenting the object region within the box [10, 15, 22, 36, 37]. Recently, spurred by related 2D work [5, 6], the transformer design [31] has also been applied for the purpose of segmenting 3D instances [29, 30]. Other methods present weakly-supervised alternatives to methods that use dense annotations in order to lower the cost of annotating 3D data [7, 16, 35]. While all these methods aim to improve the quality of 3D instance segmentation, they are trained on a known set of semantic labels. On the other hand, our proposed method aims at segmenting objects with both known and unknown class labels.

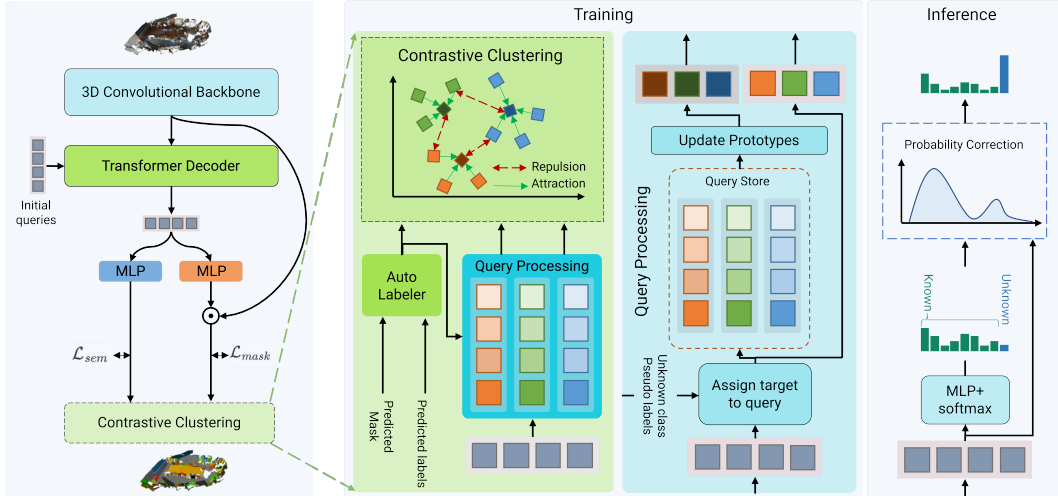


Figure 2: Proposed open-world 3D instance segmentation pipeline. From left to right: 3D instance segmentation model, where the point cloud goes through a 3D convolutional backbone. The extracted feature maps are used in the transformer decoder to refine some initial queries, which then pass through two MLPs to generate label and mask predictions. The Contrastive Clustering block takes the refined queries, the prediction masks, and labels to further process the queries by assigning a target or an *unknown* pseudo label in the Query Processing module, and then storing them in a Query Store to finally update the class prototypes, which are finally used for contrastive clustering. During inference, the queries are used to correct the probability of the predicted labels based on their reachability to the *known* class prototypes.

Open-world object recognition: Open-world object recognition was introduced in [2], where the Nearest Mean Classifier was extended for an open-world setting. In the direction of open-world object detection, many studies [41, 18, 11, 25] have been conducted in the past. In [18], pseudo-labels for the unknowns are generated to perform contrastive clustering during training for a better unknown-known classes separation, where an energy-based unknown class identifier was proposed to detect the unknown classes, based on the energy of the logits from the known classes. For incremental learning, they adopted exemplar replay to alleviate catastrophic forgetting of old classes. In the same task as [18], [11] used a transformer-based model and proposed another way of unknown pseudo-labels generation, by using a new method of objectness estimation, and introduced a foreground objectness branch that separates the background from the foreground. For the task of outdoor 3D point cloud semantic segmentation, [3] proposed a model that predicts old, novel, and unknown classes from three separate classification heads. The latter is trained on the labels of the known classes and pseudo-labels for old classes generated by the same model to alleviate catastrophic forgetting, while the unknown class is assigned the second-highest score for a better unknown class segmentation. Other methods proposed in [40, 12, 39], primarily focus on enhancing the generalizability of 3D models for novel classes by leveraging supervision from 2D Vision Language Models for object recognition and 3D semantic segmentation tasks. However, these approaches exhibit several limitations, including (i) The 3D model’s performance becomes dependent on the 2D Vision Language model. (ii) The 3D geometric properties of unseen objects in the training data are neglected during the training process. (iii) There exists no avenue for enhancing the model’s performance on novel classes in cases where new labels are introduced. (iv) The training process necessitates pairs of images and corresponding 3D scenes.

3 Closed-world 3D Instance Segmentation

We adopted the state-of-the-art 3D instance segmentation model Mask3D [29] as our baseline. The latter is a hybrid model that combines Convolutional Neural Networks (CNNs) with transformers to learn class-agnostic masks and labels for instance separation. The backbone of Mask3D is CNN-based and used to extract feature maps from multiple levels. Meanwhile, the decoder is transformer-based and used to refine $n_Q \in \mathbb{N}$ instance queries $Q = \{q_j \in \mathbb{R}^D \mid j \in (1, \dots, n_Q)\}$, using the extracted

feature maps. The learning scheme consists of a Cross-entropy loss for learning semantic class labels and binary cross-entropy loss for learning instance masks during training.

4 Open-World 3D Instance Segmentation

4.1 Problem formulation

We start by formulating the problem setting of open-world 3D instance segmentation. At a Task \mathcal{T}^t , there exists a set of *known* object categories $\mathcal{K}^t = \{1, 2, \dots, C\}$ and a set of *unknown* object categories $\mathcal{U}^t = \{C + 1, \dots\}$ that may exist on inference time. The training dataset $\mathcal{D}^t = \{\mathbf{X}^t, \mathbf{Y}^t\}$ includes samples from the classes \mathcal{K}^t . The input set $\mathbf{X}^t = \{\mathbf{P}_1, \dots, \mathbf{P}_M\}$ is made of M point clouds, where $\mathbf{P}_i \in \mathbb{R}^{N \times 3}$ is a quantized point cloud of N voxels each carrying average RGB color of the points within. The corresponding labels are $\mathbf{Y}^t = \{\mathbf{Y}_1, \dots, \mathbf{Y}_M\}$, where $\mathbf{Y}_i = \{\mathbf{y}_1, \dots, \mathbf{y}_k\}$ encodes k object instances. Each object instance $\mathbf{y}_i = [\mathbf{B}_i, l_i]$ represents a binary mask $\mathbf{B}_i \in \{0, 1\}^N$ and a corresponding class label $l_i \in \mathcal{K}^t$.

In our problem setting, \mathcal{M}_C is a 3D instance segmentation model that is trained on C object categories, and, on test time, can recognize instances from these classes, in addition to instances from new classes not seen during training by classifying them as *unknown*. The detected *unknown* instances can be used by a human user to identify a set of n new classes not previously trained on, which can be incrementally added to the learner that updates itself to produce \mathcal{M}_{C+n} without explicitly retraining on previously seen classes. At this point in Task \mathcal{T}^{t+1} , the *known* class object categories are $\mathcal{K}^{t+1} = \mathcal{K}^t \cup \{C + 1, \dots, C + n\}$. This process repeats throughout the lifespan of the instance segmentation model, continuously improving itself by incorporating new information from new classes until it reaches its maximum capacity of classes it can learn. In the rest of the paper, We assign the *unknown* class a label **0**.

4.2 Open-world scenarios

In order to simulate different realistic scenarios that might be encountered in an open-world, we propose three different ways of grouping classes under three tasks. These scenarios split scenes based on the inherent distribution (frequency-based) of object classes, the various classes encountered during the exploration of various indoor areas (region-based), and the randomness aspect of object classes in the open world.

Table 1: **The statistics of each split across the three tasks.** The number of known classes per task is reported along with the count of instances (3D objects) in the training and validation set, we also show the number of non-empty scenes used during training and validation.

	Split A			Split B			Split C		
	Task 1	Task 2	Task 3	Task 1	Task 2	Task 3	Task 1	Task 2	Task 3
Classes count	64	68	66	73	55	70	66	66	66
Train instances	24224	3791	1612	15327	8177	6123	13483	8239	7905
Validation instances	6539	1000	428	4177	2261	1529	3776	2102	2089
Train scenes	1201	924	627	1201	1002	895	1169	1089	1159
Validation scenes	312	242	165	312	264	236	307	273	300

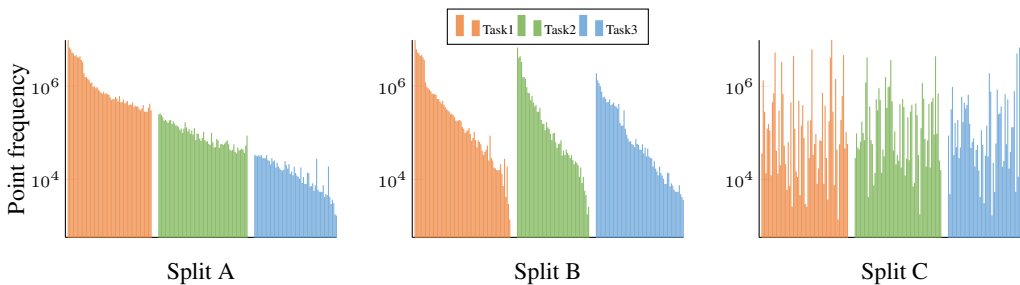


Figure 3: Point-wise count for each class across the three tasks under the three open-world scenarios

Split A (Instance frequency-based): We introduce a split that leverages the inherent distribution of objects, with *known* classes being more prevalent than *unknown* categories. Task \mathcal{T}^1 encompasses all the head classes as defined in the ScanNet200 benchmark [8, 27], while tasks \mathcal{T}^2 and \mathcal{T}^3 group the common and tail classes, respectively. This division allows us to effectively capture the varying frequency and significance of object categories within the dataset.

Split B (Region-based): In this split, our objective is to replicate the diverse class types encountered during indoor exploration. We argue that a perfect model for a robot moving indoors should segment both classes it knows and classes it hasn't seen before. Additionally, it should keep learning and getting better at segmenting new classes over time. This partition draws inspiration from the sequence of classes that a robot might encounter when navigating indoors. To achieve this, we group classes that are likely to be encountered initially when accessing an indoor space and share similarities in scenes. Initially, we assign each class to a specific scene where it predominantly occurs. Subsequently, we divide the classes into three distinct groups, corresponding to the three tasks.

Split C (Random sampling of classes): This third split introduces a different challenge inspired by the randomness aspect of the open-world, where tasks can exhibit random levels of class imbalance. To create this split, we randomly shuffled the classes and sampled without replacement, selecting 66 classes three times for each task.

4.3 Generating pseudo-labels for the unknown classes

Because of the wide range of classes in an open-world setting, the auto-labeler is used as an alternative to manual labeling. The former makes use of the existing target labels from the available ground truth classes (*known* classes) to generate pseudo-labels for the *unknown* class in the process of training. In [18], the model is assumed to be class agnostic, where *unknown* objects are predicted as *known* with high confidence. As a result, the authors of the paper proposed to use the predictions with top-k confidence scores that do not intersect with the ground truth as pseudo-labels for the *unknown* class. In our study, we show that top-k pseudo-label selection can severely harm the performance of the model on the *known* and *unknown* classes. Hence, we propose a Confidence Thresholding (CT) based selection of pseudo-labels. We show that the performance on the *known* and the *unknown* classes increases by a large margin in terms of mean Average Precision (mAP).

The *auto-labeler* unit, depicted in Fig. 2, is used for *unknown* pseudo-labels generation. It takes a set of predicted binary masks $\mathbf{B} = \{\mathbf{B}_i \mid i \in (1, \dots, n_Q)\}$, where n_Q is the number of queries, $\mathbf{B}_i = \mathbb{1}(M_i > 0.5)$ is a mask from a single query, and $M_i = \{m_{i,j} \in [0, 1] \mid j \in (1, \dots, N)\}$ is a heat map measuring the similarity between a query $q_j \in \mathbb{R}^D$ and the features of N voxels extracted from the high-resolution level in the backbone.

Moreover, each query q_j encodes semantic information and can generate a class prediction $\mathbb{P}_{cls}(q_j) = \{\mathbb{P}_{cls}(c; q_j) \mid c \in (0, 1, \dots, |\mathcal{K}^t|)\}$ using a classification head (refer to Fig. 2). Subsequently, the objectness confidence score is assigned to predictions following Eq 1.

$$s_j = s_{cls,j} \cdot \frac{M_j \cdot \mathbb{1}(M_j > 0.5)^T}{|\mathbb{1}(M_j > 0.5)|_1} \quad (1)$$

where $s_{cls,j} \in \mathbb{R}$ is the max output probability from the classification head $\mathbb{P}_{cls}(q_j)$, and $\mathbb{1}$ is the indicator function. After scoring the predictions, the auto-labeler returns m pseudo-labels $\tilde{\mathbf{Y}} = \{\tilde{\mathbf{y}}_i = [\tilde{\mathbf{B}}_i, \mathbf{0}] \mid i \in (1, \dots, m)\}$ with confidence above a threshold and has a low IoU with the *known* classes' target masks.

4.4 Query target assignment and contrastive clustering

Similar to [18], we utilize contrastive clustering to enhance the separation of classes within the query embedding space. To achieve this, we employ a set of query prototypes denoted as $\mathcal{Q}_p = \{\mathbf{q}_i \in \mathbb{R}^D \mid i \in (0, 1, \dots, |\mathcal{K}^t|)\}$, where \mathbf{q}_0 denotes the prototype of the class *unknown*. We apply a contrastive loss that encourages queries with similar classes to be attracted to their respective prototypes while pushing them away from those representing negative classes, as illustrated in Fig. 2. Since the queries are used to determine the class of the objects (see Fig. 2 inference block), the class prototypes are expected to hold general semantic knowledge of their corresponding classes.

Hungarian matching is performed in the *Assign target to query* module, depicted in Fig. 2, where the indices of prediction-target are used to assign a label to the queries used to generate the matched prediction. The labeled queries are then stored in a *query store* \mathcal{Q}_{store} , which represents a queue with a maximum capacity. This queue is employed to update the query prototypes \mathcal{Q}_p using an exponential moving average.

Hinge embedding loss is utilized according to Eq 2. This loss ensures that queries belonging to the same class denoted as q_c , are pulled towards their corresponding class prototype \mathbf{q}_c , while being pushed away from other prototypes representing different classes.

$$\mathcal{L}_{cont}(q_c) = \sum_{i=0}^{|\mathcal{K}^t|} \ell(q_c, \mathbf{q}_i) \quad (2)$$

$$\ell(q_c, \mathbf{q}_i) = \begin{cases} \|q_c - \mathbf{q}_i\|_2 & i = c \\ \max(0, \Delta - \|q_c - \mathbf{q}_i\|_2) & i \neq c \end{cases}$$

where Δ is the margin of the contrastive clustering.

4.5 Reachability-based probability correction (PC)

In [23], an architecture that can deal with long-tail distribution and *unknown* class prediction for open-world object recognition was proposed, where *unknown* classes are assumed to be very different in color and texture from the *known* classes without prior on the *unknown* classes. However, we show in Fig. 6 that many *unknown* instances hold similar features to the *known* ones.

In our method, we relax the strict assumption of high dissimilarity of *unknown* and *known* classes and correct the predicted output probability following two characteristics of a feature from an *unknown* object: (1) it has to be far from the nearest *known* class, as features of the class *unknown* are expected to be pushed away from the prototypes of the *known* classes, after applying constructive clustering, and (2) the feature should correspond to an object that is not a *known* class. We show that applying this approach during inference boosts the performance of the model on the *unknown* class considerably by compensating for the weak pseudo-labels provided by the auto-labeler.

Our probability correction scheme is the following

$$\mathbb{P}(\mathbf{0}; q_j) = \mathbb{P}_{cls}(\mathbf{0}; q_j) \cup \mathbb{P}_{corr}(\mathbf{0}; q_j) \quad (3)$$

where \mathbb{P}_{cls} is the probability from the classification head, and \mathbb{P}_{corr} is the correction probability. We base our intuition on the fact that *unknown* classes have high objectness scores, which makes them not too far from the prototypes of the *known* classes. To model this behavior we choose

$$\mathbb{P}_{corr}(\mathbf{0}; q_j) = \mathbb{P}_{corr}(\mathbf{0}; o, q_j) \cdot \mathbb{P}_{corr}(o; q_j)$$

where $\mathbb{P}_{corr}(o; q_j)$ is the likelihood of the query to correspond to an object that is not *known* (either background or true *unknown*). Since the query prototypes encode class-specific information we propose the following method to measure the objectness of a query given all prototypes from the *known* classes, where it assigns a high objectness probability if it is close to only a few *known* classes. This probability distribution defines the objectness of *unknown* objects around a certain boundary from the prototypes as follows.

$$\mathbb{P}_{corr}(o; q_j) = 1 - \sum_{k=1}^{|\mathcal{K}^t|} \mathbb{P}_{cls}(k; q_j)$$

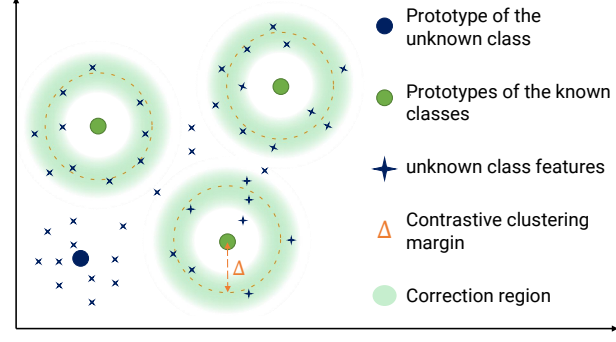


Figure 4: Illustration of the region in the query embedding space where the class probability is corrected.

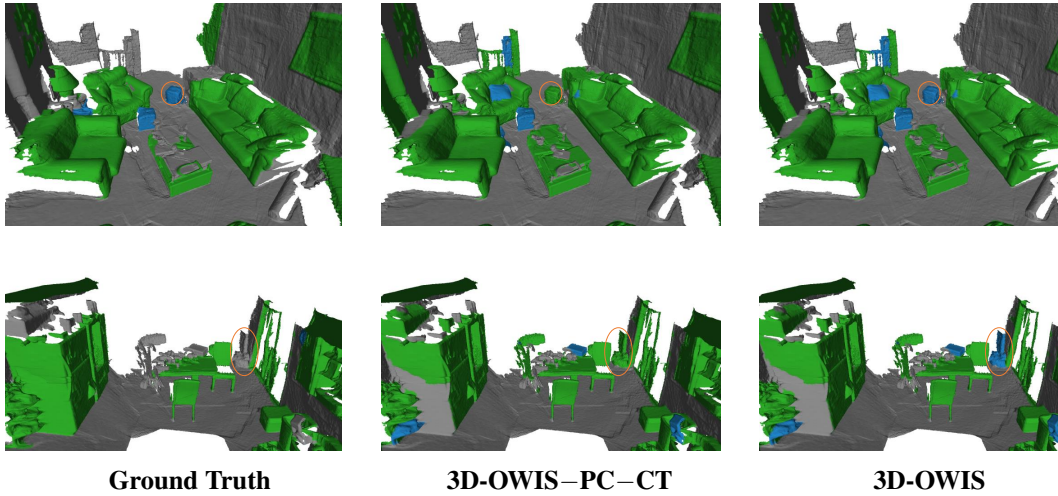


Figure 5: **Qualitative results for 3D instance segmentation results on some ScanNet200 validation scenes.** Points highlighted in blue belong to *unknown* classes and those highlighted in green belong to *known* classes. We show the performance of our model in retrieving the *unknown* class objects compared to **3D-OWIS-PC-CT** for the three scenes.

while $\mathbb{P}_{corr}(\mathbf{0}; o, q_j)$ is the probability of the query being an *unknown* object, which has a high value the further it is from the nearest prototype of the *known* classes.

$$\mathbb{P}_{corr}(\mathbf{0}; o, q_j) = \sigma\left(\frac{\gamma(q_j) - a}{b}\right); \quad \gamma(q_j) = \min_{\mathbf{q}_i} \|\mathbf{q}_j - \mathbf{q}_i\|_2$$

Here σ is the sigmoid function, $\gamma(q_j)$ is the reachability of the query q_j , \mathbf{q}_i is the prototype of the i^{th} class, and a, b are the shift and scale of the sigmoid function that assure $\mathbb{P}_{corr}(\mathbf{0}; o, q_j, \gamma(q_j) = 0) = 0.05$ and $\mathbb{P}_{corr}(\mathbf{0}; o, q_j, \gamma(q_j) = \frac{\Delta}{2}) = 0.95$, for a contrastive clustering margin Δ .

We finally normalize the probabilities from the classification head of the *known* classes as follows

$$\mathbb{P}(c; q_j) = \frac{\mathbb{P}_{cls}(c; q_j)}{\sum_{l \in \mathcal{K}^t} \mathbb{P}_{cls}(l; q_j)} (1 - \mathbb{P}(\mathbf{0}; q_j))$$

4.6 Alleviating catastrophic forgetting for incremental learning

Following the success of exemplar replay in avoiding catastrophic forgetting of the old classes during incremental learning for object detection [18, 11, 41], we adopt it for the task of incremental learning in 3D instance segmentation where we use exemplars from the classes of the previous task to fine-tune the model trained on the novel classes. In our setting, we use the same dataset for the three tasks and mask the classes of the previous task when training on the novel classes from the current task. As a result, the novel classes of the current task might be encountered again when replaying the exemplars from the previous task, as the same scenes are being used in fine-tuning.

5 Experiments

5.1 Open-world evaluation protocol

We use our proposed splits of classes which mimic the challenges that are mostly faced in the open-world to ensure a strict performance evaluation for 3D instance segmentation models.

Evaluation metrics. We adopt three common evaluation metrics, *wilderness impact* (WI) [9], *absolute open set error* (A-OSE) [26], and the *recall of the unknown classes* (U-Recall) [1, 24, 11]

Table 2: **State-of-the-Art comparison for 3D-OWIS model.** We show a comparison of performance under the three open-world scenarios, where **3D-OWIS–PC – CT** is our model **3D-OWIS** without Probability Correction (**PC**) and Confidence Thresholding (**CT**). We rely on the metrics used in the open-world literature, **A-OSE** which quantifies the number of unknown objects misclassified as one of the known classes, **WI** which measures the impact of the unknown class on the precision of the model on the known classes, and the **U-Recall** to evaluate the model’s ability to recover the unknown objects. We show that **3D-OWIS** performs remarkably better than the other models under all scenarios when dealing with the known classes, and superior performance in split A and B, and slightly less performance in split C when handling the unknown objects. We also provide a closed-setting comparison between Mask3D and Oracle (**Ours** with access to unknown labels).

Task IDs (→)	Task 1							Task 2							Task 3							
	WI			A-OSE		U-Recall		mAP (↑)		WI			A-OSE		U-Recall		mAP (↑)		mAP (↑)			
	(↓)	(↓)	(↑)	Current known	All	Current known	All	(↓)	(↓)	(↑)	Previously known	Current known	All	(↓)	(↓)	(↑)	Previously known	Current known	All			
Split A																						
Oracle	0.129	227	55.94	38.75	38.60	0.03	112	45.40	38.25	20.91	29.40	29.58	17.78	26.10	-	-	-	-	-	-	-	
Mask3D [29]	-	-	-	39.12	39.12	-	-	-	38.30	20.57	29.15	28.61	18.33	25.58	-	-	-	-	-	-	-	
3D-OW-DETR [11]	0.547	721	22.14	35.56	35.05	0.282	253	26.24	18.18	13.62	15.76	21.56	08.38	17.67	-	-	-	-	-	-	-	
3D-OWIS–PC – CT	1.589	707	30.72	37.50	37.00	0.000	4	04.75	11.00	17.30	14.10	21.40	08.00	17.50	-	-	-	-	-	-	-	
Ours: 3D-OWIS	0.397	607	34.75	40.2	39.7	0.007	126	27.03	29.40	16.40	22.70	20.20	15.20	18.70	-	-	-	-	-	-	-	
Split B																						
Oracle	1.126	939	70.31	24.57	24.80	0.180	441	73.16	25.50	20.30	23.40	23.40	30.40	26.00	-	-	-	-	-	-	-	-
Mask3D [29]	-	-	-	23.48	23.48	-	-	-	21.81	18.91	20.37	24.20	29.22	26.06	-	-	-	-	-	-	-	-
3D-OW-DETR [11]	3.229	1935	17.18	20.00	19.73	0.203	1389	33.31	12.36	13.86	12.93	07.27	18.96	11.62	-	-	-	-	-	-	-	-
3D-OWIS–PC – CT	3.133	1895	21.67	18.94	18.70	3.169	1081	26.63	18.00	16.40	17.20	17.30	20.10	18.30	-	-	-	-	-	-	-	-
Ours: 3D-OWIS	3.684	1780	24.79	23.60	23.30	0.755	581	24.21	18.70	17.30	17.90	18.70	24.60	20.90	-	-	-	-	-	-	-	-
Split C																						
Oracle	1.039	651	71.61	23.30	23.6	0.249	591	62.83	20.50	18.40	19.60	25.30	28.20	26.30	-	-	-	-	-	-	-	-
Mask3D [29]	-	-	-	20.82	21.15	-	-	-	22.67	26.67	24.13	25.41	25.21	25.35	-	-	-	-	-	-	-	-
3D-OW-DETR [11]	1.463	1517	13.00	14.81	14.59	1.330	847	16.04	08.00	17.41	12.40	08.81	15.63	11.01	-	-	-	-	-	-	-	-
3D-OWIS–PC – CT	2.901	1752	15.66	15.00	14.80	1.799	666	15.99	13.50	19.70	16.40	17.50	17.70	17.50	-	-	-	-	-	-	-	-
Ours: 3D-OWIS	0.419	1294	14.34	18.00	17.60	0.152	303	15.80	13.90	22.20	17.80	17.80	17.70	17.80	-	-	-	-	-	-	-	-

to evaluate the performance of our model on the *unknown* classes and to provide a fair comparison with and without contributions. For the *known* classes, we use mean Average Precision (mAP). WI measures the impact of the *unknown* classes on the precision of the model at a specific confidence level. Ideally, WI is nil, i.e., there are no *unknown* objects predicted as *known*. For our evaluation, we report WI at 0.5 confidence. It can be computed as follows: $WI = \frac{P_{K|U}}{P_{K|U} + P_{K|U}} - 1$.

We also report A-OSE, which represents the count of *unknown* instances misclassified as one of the *known* classes, and the U-Recall at 0.5 IoU, which reflects the ability of the model to recover *unknown* objects.

5.2 Implementation details

We adapt Mask3D [29] for the task of open-world instance segmentation. We add an extra prediction output for the *unknown* class. In training, we assign an *ignore* label to the classes of the future and previous tasks, while we keep the labels of the previous task and assign an *unknown* class label to the classes of the future task during evaluation. For contrastive clustering, we use the indices obtained after matching the predictions with the target using *Hungarian matching* to assign a label to the queries and store them in the *Query Store* Q_{store} . The store is then averaged per class and used to periodically update the prototypes every 10 iterations for the hinge loss computation. Finally, we use 40 exemplars per class on average for incremental learning. The classes from the current task are kept during class exemplar replay since we are using the same dataset for the three tasks.

5.3 Open-world results

Table 2 provides a comprehensive performance comparison between the Oracle, our implementation of [11] as 3D-OW-DETR, **3D-OWIS**, and **3D-OWIS–PC – CT** when excluding the Probability Correction (**PC**) and Confidence Thresholding (**CT**) components. Across all scenarios and tasks,

Table 3: **Extensive ablation of the added components.** We perform the ablation by adding Probability Correction (**PC**) and Confidence Thresholding (**CT**) components to **3D-OWIS-PC – CT**. We conduct the performance comparison in terms of mAP, U-Recall, WI, and A-OSE. Even though **3D-OWIS** is performing well in retrieving the *unknown* classes without **PC** and **CT**, which is reflected by the high U-Recall, it is still performing poorly on the *known* classes, based on the high WI and A-OSE. This negative impact on the *known* classes accumulates over the tasks and results in further reduction in mAP. When adding the **CT**, the performance on the *known* classes improves considerably and remains consistent throughout the incremental learning process. Probability correction (**PC**) significantly improves the U-Recall in all cases. Even though the latter shows lower performance in terms of WI and A-OSE, the overall mAP slightly improves or remains higher with a large margin compared **3D-OWIS-PC – CT**. This shows that adding **PC** and **CT** gives the best compromise in performance on both *known* and *unknown* classes.

w/ Finetuning	Task IDs (→)			Task 1						Task 2						Task 3		
	CT	PC		WI	A-OSE	U-Recall	mAP (↑)		WI	A-OSE	U-Recall	mAP (↑)		WI	A-OSE	U-Recall	mAP (↑)	
				(↓)	(↓)	(↑)	Current known	All	(↓)	(↓)	(↑)	Previously known	Current known	All	Previously known	Current known	All	Previously known
Split A																		
×	×	×		1.589	707	30.72	37.50	37.00	0.870	321	19.42	00.00	16.74	08.40	00.00	09.30	02.80	
×	✓	✗		0.237	443	30.00	40.30	39.70	0.306	129	14.96	00.00	21.00	10.50	00.00	17.45	05.20	
✓	✗	✗		1.589	707	30.72	37.50	37.00	0.000	4	04.75	11.00	17.30	14.10	21.40	08.00	17.50	
✓	✓	✗		0.237	443	30.00	40.30	39.70	0.004	102	23.62	29.22	15.80	22.30	19.70	15.70	18.50	
✓	✓	✓		0.398	607	34.75	40.2	39.70	0.007	126	27.03	29.40	16.40	22.70	No unknown labels for evaluation			
Split B																		
×	✗	✗		3.133	1895	21.67	18.94	18.70	1.82	829	17.20	00.00	15.40	06.60	00.00	20.20	07.50	
×	✓	✗		2.147	21.70	21.70	23.80	23.50	1.563	375	13.08	00.00	18.30	07.90	00.00	25.40	09.40	
✓	✗	✗		3.219	1905	21.70	18.94	18.70	3.169	1081	26.63	18.00	16.40	17.20	17.30	20.10	18.30	
✓	✓	✗		2.147	1397	21.70	23.80	23.50	0.466	413	20.90	18.60	16.90	17.70	18.50	24.20	20.60	
✓	✓	✓		3.684	1780	24.79	23.6	23.30	0.755	581	24.21	18.70	17.30	17.90	No unknown labels for evaluation			
Split C																		
×	✗	✗		2.901	1752	15.66	15.00	14.80	6.294	857	11.05	0.00	15.70	07.50	00.00	14.60	04.70	
×	✓	✗		0.227	828	11.44	18.70	18.40	1.361	365	10.16	00.00	19.50	09.40	00.00	19.10	6.20	
✓	✗	✗		2.901	1752	15.66	15.00	14.80	1.799	666	15.99	13.50	19.70	16.40	17.50	17.70	17.50	
✓	✓	✗		0.227	828	11.44	18.70	18.40	0.088	208	12.63	14.50	22.10	18.00	17.80	17.70	17.80	
✓	✓	✓		0.419	1294	14.34	18	17.60	0.152	303	15.80	13.90	22.20	17.80	No unknown labels for evaluation			

3D-OWIS-PC – CT consistently exhibits inferior performance in terms of mAP. Additionally, it demonstrates considerably lower U-Recall performance in splits A and B, with slightly higher

performance in split C. Of particular note, our **3D-OWIS** demonstrates remarkable proficiency in preserving knowledge of the previous classes after fine-tuning. This proficiency is attributed to better pseudo-label selection for the *unknown* classes. **3D-OWIS** outperforms **3D-OWIS-PC – CT** in most cases while minimizing the impact of the *unknown* classes on the *known* classes, as evidenced by lower WI and A-OSE scores and higher mAP.

Table 4 presents a comparison between our model, **3D-OWIS**, and our implementation of two methods, GGN [32] and OLN [19]. For both models, we adapt Mask3D and train it with mask loss only for OLN. In the case of GGN, we train a Minkowski backbone to predict affinity maps and use Connected Components to generate class-agnostic proposals. These results underscore the effectiveness and potential of our approach in addressing the three proposed open-world challenges.

5.4 Incremental learning results

Our model’s performance in incremental learning is evaluated based on its ability to preserve knowledge from previous classes. With the utilization of exemplar replay, the **3D-OWIS** model demonstrates significant improvement on previous classes mAP. Table 2 presents the results, indicating that our model consistently outperforms the others in terms of mean Average Precision (mAP) for the previous classes in all cases.

5.5 Discussion and analysis

Ablation study. We show in Table 3 that **3D-OWIS-PC – CT** model performs poorly on the *known* classes because of the high number of low-quality pseudo-labels generated by *Auto-labeler*, which is also explained by the high value of *Wilderness Impact* and *Absolute open set error*. The U-Recall drops considerably when fine-tuning the **3D-OWIS-PC – CT**, while the WI and A-OSE either decrease or increase with the mAP on the *unknown*. On the other hand, our model limits the training only to the best pseudo-labels, which maintain good performance on the *known* classes in all cases, before and after fine-tuning, and also achieve results on the *unknown* class comparable to the **3D-OWIS-PC – CT** in most of the cases. Adding the probability correction module helps in improving the U-Recall while keeping the mAP of the *known* classes much above the **3D-OWIS-PC – CT**. However, it results in an increase in WI and A-OSE because of the increase of false positives in the *known* classes.

tSNE analysis The tSNE plot shown in Fig. 6 illustrates the below-par performance of the **3D-OWIS-PC – CT** in clustering the *unknown* classes, where most queries are still maintaining features representative of the *known* classes. This behavior is a result of the weak supervision of the *unknown* class, which shows the need for correcting the predictions, and explains the improvement in U-Recall when applying the probability correction with nil deterioration in the *known* classes mAP in most cases.

Qualitative analysis. Fig. 5 shows that 3D-OWIS is able to correctly identify background and *unknown* objects as *unknown*. Also note the second scene, where predictions are corrected from *known* to *unknown* without affecting the predictions of the *known* classes.

6 Limitations

Confidence Thresholding (**CT**) enhances the performance of the model on *known* classes; nonetheless, it diminishes the model’s capacity to segment *unknown* classes, mainly due to its reliance on a smaller number of pseudo-labels during training. Additionally, the effectiveness of Probability Correction (**PC**) is contingent upon the inherent characteristics of the clusters within the *known* classes. In scenarios characterized by data imbalance, the performance of probability correction may deteriorate when applied to the undersampled classes.

7 Conclusion

In this paper, we address the challenge of 3D instance segmentation in open-world scenarios, which is a novel problem formulation. We propose an innovative approach that incorporates an *unknown* object identifier to detect objects not present in the training set. To facilitate evaluation and experimentation, we present three dataset splits of ScanNet200 based on different criteria for selecting *unknown* objects. Our experimental results demonstrate that our proposed *unknown* object identifier significantly improves the detection of *unknown* objects across various tasks and dataset splits. This work contributes to advancing the localization and segmentation of 3D objects in real-world environments and paves the way for more robust and adaptable vision systems.

Table 4: **Open-world instance segmentation comparison.** We provide the results of our implementation of two methods for 2D open-world instance segmentation models. We show that our model performs comparatively better than others across all metrics.

Task ID	Split A					
				Task 1		
	WI (↓)	A-OSE (↓)	U-Recall (↑)	mAP (↑) Current known	mAP (↑) All	
3D-GGN [32]	15.68	1452	21.33	20.51	20.12	
3D-OLN [19]	-	-	02.45	-	-	
Ours: 3D-OWIS	0.397	607	34.75	40.2	39.7	

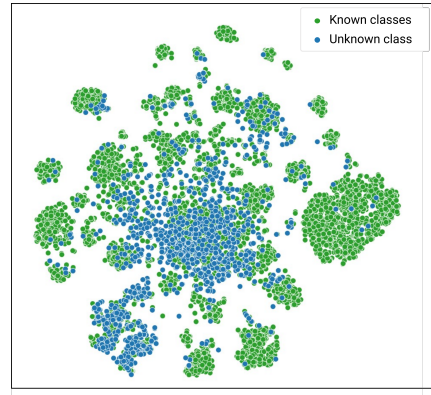


Figure 6: **tSNE visualization** of the queries for *known* & *unknown* classes

Acknowledgement The computational resources were provided by the National Academic Infrastructure for Supercomputing in Sweden (NAISS), partially funded by the Swedish Research Council through grant agreement No. 2022-06725, and by the Berzelius resource, provided by Knut and Alice Wallenberg Foundation at the National Supercomputer Center.

References

- [1] A. Bansal, K. Sikka, G. Sharma, R. Chellappa, and A. Divakaran. Zero-shot object detection. In *Proceedings of the European Conference on Computer Vision (ECCV)*, pages 384–400, 2018. [7](#)
- [2] A. Bendale and T. Boult. Towards open world recognition. In *Proceedings of the IEEE conference on computer vision and pattern recognition*, pages 1893–1902, 2015. [3](#)
- [3] J. Cen, P. Yun, S. Zhang, J. Cai, D. Luan, M. Tang, M. Liu, and M. Yu Wang. Open-world semantic segmentation for lidar point clouds. In *Computer Vision–ECCV 2022: 17th European Conference, Tel Aviv, Israel, October 23–27, 2022, Proceedings, Part XXXVIII*, pages 318–334. Springer, 2022. [3](#)
- [4] S. Chen, J. Fang, Q. Zhang, W. Liu, and X. Wang. Hierarchical aggregation for 3d instance segmentation. In *Proceedings of the IEEE/CVF International Conference on Computer Vision*, pages 15467–15476, 2021. [2](#)
- [5] B. Cheng, I. Misra, A. G. Schwing, A. Kirillov, and R. Girdhar. Masked-attention mask transformer for universal image segmentation. In *Proceedings of the IEEE/CVF Conference on Computer Vision and Pattern Recognition*, pages 1290–1299, 2022. [2](#)
- [6] B. Cheng, A. Schwing, and A. Kirillov. Per-pixel classification is not all you need for semantic segmentation. *Advances in Neural Information Processing Systems*, 34:17864–17875, 2021. [2](#)
- [7] J. Chibane, F. Engelmann, T. Anh Tran, and G. Pons-Moll. Box2mask: Weakly supervised 3d semantic instance segmentation using bounding boxes. In *Computer Vision–ECCV 2022: 17th European Conference, Tel Aviv, Israel, October 23–27, 2022, Proceedings, Part XXXI*, pages 681–699. Springer, 2022. [2](#)
- [8] A. Dai, A. X. Chang, M. Savva, M. Halber, T. Funkhouser, and M. Nießner. Scannet: Richly-annotated 3d reconstructions of indoor scenes. In *Proceedings of the IEEE conference on computer vision and pattern recognition*, pages 5828–5839, 2017. [5](#)
- [9] A. Dhamija, M. Gunther, J. Ventura, and T. Boult. The overlooked elephant of object detection: Open set. In *Proceedings of the IEEE/CVF Winter Conference on Applications of Computer Vision*, pages 1021–1030, 2020. [7](#)
- [10] F. Engelmann, M. Bokeloh, A. Fathi, B. Leibe, and M. Nießner. 3d-mpa: Multi-proposal aggregation for 3d semantic instance segmentation. In *Proceedings of the IEEE/CVF conference on computer vision and pattern recognition*, pages 9031–9040, 2020. [2](#)
- [11] A. Gupta, S. Narayan, K. Joseph, S. Khan, F. S. Khan, and M. Shah. Ow-detr: Open-world detection transformer. In *Proceedings of the IEEE/CVF Conference on Computer Vision and Pattern Recognition*, pages 9235–9244, 2022. [1, 3, 7, 8](#)
- [12] H. Ha and S. Song. Semantic abstraction: Open-world 3d scene understanding from 2d vision-language models. In *6th Annual Conference on Robot Learning*, 2022. [3](#)
- [13] L. Han, T. Zheng, L. Xu, and L. Fang. Occuseg: Occupancy-aware 3d instance segmentation. In *Proceedings of the IEEE/CVF conference on computer vision and pattern recognition*, pages 2940–2949, 2020. [2](#)
- [14] T. He, C. Shen, and A. Van Den Hengel. Dyco3d: Robust instance segmentation of 3d point clouds through dynamic convolution. In *Proceedings of the IEEE/CVF conference on computer vision and pattern recognition*, pages 354–363, 2021. [2](#)
- [15] J. Hou, A. Dai, and M. Nießner. 3d-sis: 3d semantic instance segmentation of rgb-d scans. In *Proceedings of the IEEE/CVF conference on computer vision and pattern recognition*, pages 4421–4430, 2019. [2](#)

- [16] J. Hou, B. Graham, M. Nießner, and S. Xie. Exploring data-efficient 3d scene understanding with contrastive scene contexts. In *Proceedings of the IEEE/CVF Conference on Computer Vision and Pattern Recognition*, pages 15587–15597, 2021. [2](#)
- [17] L. Jiang, H. Zhao, S. Shi, S. Liu, C.-W. Fu, and J. Jia. Pointgroup: Dual-set point grouping for 3d instance segmentation. In *Proceedings of the IEEE/CVF conference on computer vision and Pattern recognition*, pages 4867–4876, 2020. [2](#)
- [18] K. Joseph, S. Khan, F. S. Khan, and V. N. Balasubramanian. Towards open world object detection. In *Proceedings of the IEEE/CVF Conference on Computer Vision and Pattern Recognition*, pages 5830–5840, 2021. [1](#), [3](#), [5](#), [7](#)
- [19] D. Kim, T.-Y. Lin, A. Angelova, I. S. Kweon, and W. Kuo. Learning open-world object proposals without learning to classify. *IEEE Robotics and Automation Letters*, 7(2):5453–5460, 2022. [9](#), [10](#)
- [20] J. Lahoud, B. Ghanem, M. Pollefeys, and M. R. Oswald. 3d instance segmentation via multi-task metric learning. In *Proceedings of the IEEE/CVF International Conference on Computer Vision*, pages 9256–9266, 2019. [2](#)
- [21] Z. Liang, Z. Li, S. Xu, M. Tan, and K. Jia. Instance segmentation in 3d scenes using semantic superpoint tree networks. In *Proceedings of the IEEE/CVF International Conference on Computer Vision*, pages 2783–2792, 2021. [2](#)
- [22] S.-H. Liu, S.-Y. Yu, S.-C. Wu, H.-T. Chen, and T.-L. Liu. Learning gaussian instance segmentation in point clouds. *arXiv preprint arXiv:2007.09860*, 2020. [2](#)
- [23] Z. Liu, Z. Miao, X. Zhan, J. Wang, B. Gong, and S. X. Yu. Large-scale long-tailed recognition in an open world. In *Proceedings of the IEEE/CVF conference on computer vision and pattern recognition*, pages 2537–2546, 2019. [6](#)
- [24] C. Lu, R. Krishna, M. Bernstein, and L. Fei-Fei. Visual relationship detection with language priors. In *Computer Vision–ECCV 2016: 14th European Conference, Amsterdam, The Netherlands, October 11–14, 2016, Proceedings, Part I 14*, pages 852–869. Springer, 2016. [7](#)
- [25] S. Ma, Y. Wang, J. Fan, Y. Wei, T. H. Li, H. Liu, and F. Lv. Cat: Localization and identification cascade detection transformer for open-world object detection. *arXiv preprint arXiv:2301.01970*, 2023. [3](#)
- [26] D. Miller, L. Nicholson, F. Dayoub, and N. Sünderhauf. Dropout sampling for robust object detection in open-set conditions. In *2018 IEEE International Conference on Robotics and Automation (ICRA)*, pages 3243–3249. IEEE, 2018. [7](#)
- [27] D. Rozenberszki, O. Litany, and A. Dai. Language-grounded indoor 3d semantic segmentation in the wild. In *Computer Vision–ECCV 2022: 17th European Conference, Tel Aviv, Israel, October 23–27, 2022, Proceedings, Part XXXIII*, pages 125–141. Springer, 2022. [5](#)
- [28] K. Saito, P. Hu, T. Darrell, and K. Saenko. Learning to detect every thing in an open world. In *Computer Vision–ECCV 2022: 17th European Conference, Tel Aviv, Israel, October 23–27, 2022, Proceedings, Part XXIV*, pages 268–284. Springer, 2022. [1](#)
- [29] J. Schult, F. Engelmann, A. Hermans, O. Litany, S. Tang, and B. Leibe. Mask3D: Mask Transformer for 3D Semantic Instance Segmentation. In *International Conference on Robotics and Automation (ICRA)*, 2023. [2](#), [3](#), [8](#)
- [30] J. Sun, C. Qing, J. Tan, and X. Xu. Superpoint transformer for 3d scene instance segmentation. *arXiv preprint arXiv:2211.15766*, 2022. [2](#)
- [31] A. Vaswani, N. Shazeer, N. Parmar, J. Uszkoreit, L. Jones, A. N. Gomez, Ł. Kaiser, and I. Polosukhin. Attention is all you need. *Advances in neural information processing systems*, 30, 2017. [2](#)
- [32] W. Wang, M. Feiszli, H. Wang, J. Malik, and D. Tran. Open-world instance segmentation: Exploiting pseudo ground truth from learned pairwise affinity. In *Proceedings of the IEEE/CVF Conference on Computer Vision and Pattern Recognition*, pages 4422–4432, 2022. [9](#), [10](#)

- [33] W. Wang, M. Feiszli, H. Wang, and D. Tran. Unidentified video objects: A benchmark for dense, open-world segmentation. In *Proceedings of the IEEE/CVF International Conference on Computer Vision*, pages 10776–10785, 2021. [1](#)
- [34] W. Wang, R. Yu, Q. Huang, and U. Neumann. Sgpn: Similarity group proposal network for 3d point cloud instance segmentation. In *Proceedings of the IEEE conference on computer vision and pattern recognition*, pages 2569–2578, 2018. [2](#)
- [35] S. Xie, J. Gu, D. Guo, C. R. Qi, L. Guibas, and O. Litany. Pointcontrast: Unsupervised pre-training for 3d point cloud understanding. In *Computer Vision–ECCV 2020: 16th European Conference, Glasgow, UK, August 23–28, 2020, Proceedings, Part III 16*, pages 574–591. Springer, 2020. [2](#)
- [36] B. Yang, J. Wang, R. Clark, Q. Hu, S. Wang, A. Markham, and N. Trigoni. Learning object bounding boxes for 3d instance segmentation on point clouds. *Advances in neural information processing systems*, 32, 2019. [2](#)
- [37] L. Yi, W. Zhao, H. Wang, M. Sung, and L. J. Guibas. Gspn: Generative shape proposal network for 3d instance segmentation in point cloud. In *Proceedings of the IEEE/CVF Conference on Computer Vision and Pattern Recognition*, pages 3947–3956, 2019. [2](#)
- [38] B. Zhang and P. Wonka. Point cloud instance segmentation using probabilistic embeddings. In *Proceedings of the IEEE/CVF Conference on Computer Vision and Pattern Recognition*, pages 8883–8892, 2021. [2](#)
- [39] J. Zhang, R. Dong, and K. Ma. Clip-fo3d: Learning free open-world 3d scene representations from 2d dense clip. *arXiv preprint arXiv:2303.04748*, 2023. [3](#)
- [40] X. Zhu, R. Zhang, B. He, Z. Zeng, S. Zhang, and P. Gao. Pointclip v2: Adapting clip for powerful 3d open-world learning. *arXiv preprint arXiv:2211.11682*, 2022. [3](#)
- [41] O. Zohar, K.-C. Wang, and S. Yeung. Prob: Probabilistic objectness for open world object detection. In *Proceedings of the IEEE/CVF Conference on Computer Vision and Pattern Recognition*, pages 11444–11453, 2023. [3](#) [7](#)

Appendix

A Scalability of 3D-OWIS

We show in Table 5 that **3D-OWIS** can accommodate a large number of classes without a major size increase

Table 5: Demonstrating the Scalability of **3D-OWIS** with Respect to the maximum number of classes it can learn.

# of classes	200	1000	5000	10000	50000	100000
Size of 3D-OWIS	39.7M	39.8M	40.7M	41.9M	50.9M	62.2M

B Additional details on Split B

We utilize the 20 scene types present in the ScanNet200 dataset to distribute the 200 classes over the three tasks. Initially, we establish a notion of similarity between two scene types by assessing the extent of their shared classes. This similarity is quantified through the intersection over the union (*IoU*) metric, which measures the ratio of common classes to the total count of unique classes across both scenes. By employing this metric, we identify scene types that exhibit a substantial *IoU*, indicating a higher degree of similarity. The similarity matrix, depicted in Fig. 7, showcases the relationships between the 20 scene types within the ScanNet200 dataset.

Subsequently, we employed three criteria to group the classes: (i) the likelihood of encountering them first when accessing an indoor area, (ii) their affiliation with similar scene types, and (iii) the proximity in the number of known classes across tasks. By taking these factors into consideration, we arrived at the split of scenes presented in Table 6.

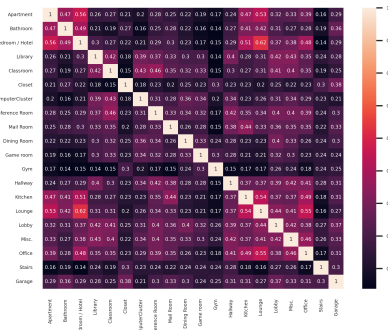


Figure 7: **Similarity matrix between the 20 scene types in ScanNet200 dataset.** We show the ratio of common classes to the total count of unique classes between two scene types.

Table 6: **Frequently occurring scene when training during the three tasks in Split B.** Scene types are grouped into tasks based on three criteria: (i) the likelihood of encountering the classes within the scene types when entering an indoor area, (ii) similarity of scene types containing the classes, and (iii) consistency in the overall number of classes within the scene types across all tasks. This grouping ensures a cohesive organization of scene types for effective evaluation of 3D instance segmentation models integrated with tasks such as robot navigation within indoor environments.

Split B						
Task 1		Task 2		Task 3		
Bedroom / Hotel	Kitchen	ComputerCluster	Mail Room	Game room	Office	
Dining Room	Bathroom	Misc.	Hallway	Apartment		
Lounge	Closet	Gym	Classroom	Lobby		
		Library	Conference Room	Stairs		

C Additional details on the experimentation

Training: We train the model on the entire ScanNet200 dataset for all tasks. In Task 1, objects belonging to the classes from Task 2 and Task 3 are masked, excluding them from the learning process. Moving to Task 2, we utilize the last saved checkpoint of the model from Task 1 as a starting point and mask the objects with labels that correspond to the current known classes of Task 1 and Task 3. This allows the model to focus solely on learning and distinguishing the specific objects associated with the current task. Finally, Task 3 builds upon the progress made in Task 2. We load the

latest checkpoint of the model from Task 2 and incorporate an exemplar replay. Similar to Task 2, the objects with labels belonging to the known classes in Task 1 and Task 2 are masked during training. This step further refines the model’s understanding and discrimination abilities for the specific objects relevant to the current task.

Evaluation: To conduct the evaluation during a task, we assign the “*unknown*” label to the known classes from all the future tasks.

D Additional qualitative results

D.1 Unknown objects identification

The qualitative results depicted in Fig. 10, 12, 13, and 11 highlight the superior performance of our contribution in retrieving unknown objects. Across the majority of scenes, our model consistently corrects the mispredicted unknown classes while preserving the accuracy of known objects, thus demonstrating its robustness and effectiveness.

D.2 Learning novel classes

Fig. 8 and Fig. 9 illustrate the sequential process of learning novel classes after identifying unknown objects from the previous task. In Fig. 8, we demonstrate the effectiveness of our method in successfully retrieving unknown classes in all tasks. Additionally, in Fig. 9, we highlight the potential of exemplar replay in retaining knowledge of the old classes after learning the novel classes in Task 2 and Task 3.

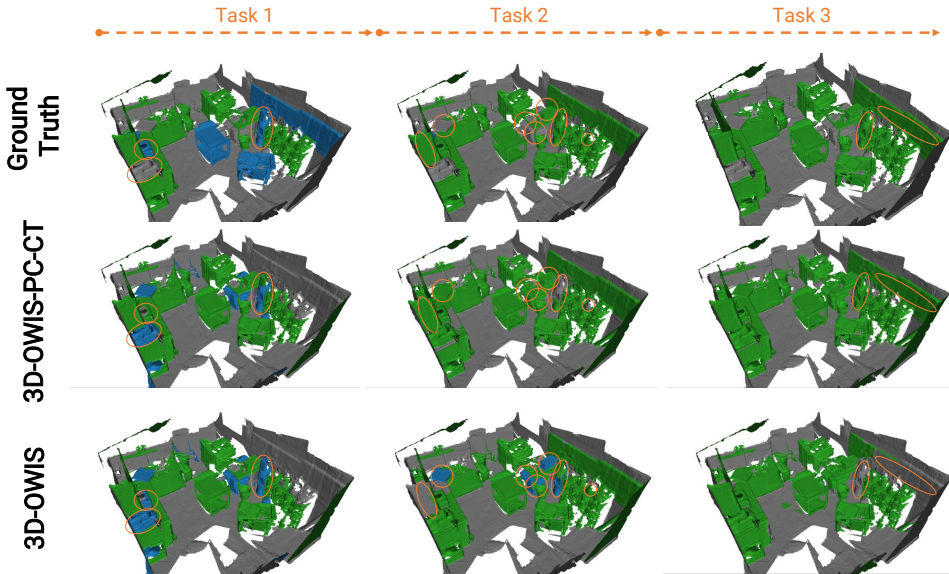


Figure 8: **Illustration of the process of unknown identification and learning novel classes.** We use orange circles to highlight the differences between **3D-OWIS** and **3D-OWIS-PC-CT**. The objects depicted in green represent the known classes, while those in blue represent the unknown objects. The gray objects correspond to the background. The qualitative results demonstrate that **3D-OWIS** outperforms **3D-OWIS-PC-CT** in retrieving unknown objects. Notably, **3D-OWIS** correctly identifies the background objects as unknown, whereas **3D-OWIS-PC-CT** misclassifies them as known objects.

Table 7: Proposed distribution of ScanNet200 classes across tasks for each split. We show the classes that are known when training the model during a specific task for the three splits.

Split A			Split B			Split C		
Task 1	Task 2	Task 3	Task 1	Task 2	Task 3	Task 1	Task 2	Task 3
tv stand	cushion	paper	alarm clock	guitar	bar	basket	ironing board	mattress
curtain	end table	plate	backpack	paper towel roll	basket	trash can	divider	toaster
blinds	dining table	soup dispenser	bag	book	bathroom cabinet	stair rail	oven	stool
shower curtain	keyboard	bucket	bed	bookshelf	bathroom counter	roaster oven	dish rack	plant
bookshelf	bag	clock	blanket	cart	bathroom stall	laundry hamper	shower door	folded chair
tv	toilet paper	guitar	case of water bottles	blackboard	bathroom stall door	bulletin board	mini fridge	microwave
kitchen cabinet	printer	toilet paper holder	ceiling	projector	bathroom vanity	dining table	bicycle	cushion
pillow	blanket	speaker	closet	seat	bathtub	stuffed animal	laptop	bench
lamp	microwave	cup	closet door	folded chair	broom	bathroom vanity	armchair	sofa dispensor
dresser	shoe	paper towel roll	closet wall	clothes	clothes dryer	box	couch	storage organizer
monitor	computer tower	bar	clothes	office chair	ceiling	coffee kettle	coffee kettle	shower curtain
obj	botle	toaster	cooker	projector screen	clips	cooker	cooker	cooker
ceiling	bin	ironing board	container	whiteboard	doorframe	pot plant	ironing board	ironing board
board	ottoman	soap dish	curtain	bin	luggage	structure	ironing board	ironing board
stove	bench	toilet paper dispenser	door	bucket	fire alarm	closet	towel	blackboard
closet wall	basket	fire extinguisher	dresser	bulleit board	hair dryer	wall	blackboard	blackboard
couch	fan	ball	dumbbell	copier	handicap bar	paper cutter	desk	desk
office chair	laptop	hat	fan	machine	ledge	paper cutter	shower curtain rod	tv
kitchen counter	person	shower curtain rod	hat	mailbox	light switch	object	sofa chair	printer
shower	paper towel dispenser	paper cutter	paper	mirror	mat	tissue box	clothes dryer	stand
closet	oven	ironing board	ironing board	paper	plate	coffee table	coffee table	rack
doorframe	rack	tray	laptop	paper	stairs	stairs	pants	bathroom counter
soft chair	piano	toaster oven	lamp	plumber	plate	toilet seat cover dispenser	toilet seat cover dispenser	toilet seat cover dispenser
mailbox	suitcase	mouse	column	scale	keyboard	closet rod	closet rod	closet rod
nightstand	mail	storage container	laptop	storage container	hat	machine	bottle	bottle
washing machine	container	scale	storage basket	bins	copier	paper bag	range hood	range hood
picture	telephone	tissue box	laundry basket	bins	shower head	book	paper	paper
book	stand	light switch	laundry hamper	structure	curtain	blinds	pinse	pinse
sink	light	crate	luggage	water bottle	shower curtain	monitor	person	person
recycling bin	laundry basket	power outlet	mattress	water bottle	shower curtain rod	shower wall	shower wall	shower wall
table	pipe	sign	mini frige	ball	paper towel dispenser	paper towel roll	coffee maker	coffee maker
backpack	seat	projector	scale	board	fire extinguisher	curtain floor	light switch	light switch
shower wall	column	candle	storage container	box	backpack	paper towel roll	curtain	curtain
toilet	bicycle	power outlet	laptop	box	shower head	closet	storage container	storage container
cooper	ladder	plunger	power outlet	cabinet	shower wall	water bottle	bathroom stall door	bathroom stall door
counter	jacket	stuffed animal	purse	cd case	sink	stove	shower floor	shower floor
stool	storage bin	headphones	rack	ceiling light	soap dish	laundry basket	kitchen cabinet	kitchen cabinet
refrigerator	coffee maker	brushon	recyeling bin	clock	dispenser	alarm clock	refrigerator	refrigerator
window	dishwasher	duspan	shelf	computer tower	toilet	beehones	fire alarm	fire alarm
file cabinet	machine	dryer	sign	cd case	toilet paper	toilet paper	fan	fan
chair	mat	storage bin	storage bin	desk	dispenser	phones	ball	ball
plant	windowsill	water bottle	storage organizer	keybord	toilet paper	alarm clock	bucket	bucket
coffee table	bulletin board	handicap bar	monitor	divider	holder	beehones	refrigerator	refrigerator
stairs	fireplace	purse	mouse	file cabinet	toilet seat cover dispenser	mirror	sign	sign
armchair	mini frige	tissue box	paper	headphones	towel	closet	toilet paper holder	toilet paper holder
cabinet	water cooler	shower floor	person	keybord	trash bin	nightstand	ceiling light	ceiling light
bathroom vanity	shower door	water pitcher	power strip	projector	washing machine	end table	end table	end table
bathroom stall	pillar	tool	strip	telephone	monitor	handicap bar	picture	picture
mirror	paper bag	bicycle	stainless	tray	closet rod	blanket	closet door	closet door
blackboard	alarm clock	candle	beam	tube	water cooler	water cooler	file cabinet	file cabinet
trash can	music stand	chair	beam	disk	pitcher	water pitcher	crat	crat
stair rail	laundry detergent	coffee table	beam	rack	dumbbell	recyeling bin	toilet paper dispenser	toilet paper dispenser
decoration	dumbbell	wardrobe	beam	stainless	furniture	lamp	pillow	pillow
box	closet door	person	beam	stainless	stuffed animal	scale	mat	mat
towel	vacuum cleaner	power strip	beam	stainless	radiatior	decoration	bathroom stall	bathroom stall
door	cd case	cd case	beam	stainless	bowel	mouse	wardrobe	wardrobe
clothes	disk	closet rod	beam	stainless	calculator	wardrobe	ottoman	ottoman
whiteboard	range hood	jacket	beam	stainless	coffee kettle	plunger	seat	seat
bed	coffee kettle	coffee kettle	beam	stainless	coffee maker	shower	power strip	power strip
bathtub	projector screen	shower head	beam	stainless	paper bag	bar	jacket	jacket
desk	divider	keybord piano	beam	stainless	plate	counter	dresser	dresser
wardrobe	bathroom counter	light	beam	stainless	power	power strip	dustpan	dustpan
clothes dryer	cost rack	music stand	beam	stainless	power	fireplace	table	table
radiator	folded chair	ottoman	beam	stainless	power	doorframe	toilet	toilet
shelf	ceiling light	piano	beam	stainless	power	toilet	trash bin	trash bin
	fire alarm	picture	beam	stainless	power	trash bin	projector	projector
	power strip	pillar	beam	stainless	power	case of water bottles	window	window
	trash bin	pillar	beam	stainless	power	light	window	window
	bathroom cabinet	potted plant	beam	stainless	power	whiteboard	tray	tray
	structure	rail	beam	stainless	power	vacuum cleaner	ed age	ed age
	storage organizer	sofa chair	beam	stainless	power	guitar case	sun dish	sun dish
	potted plant	speaker	beam	stainless	power	sink	office chair	office chair
	mattress	stool	beam	stainless	power	bathtub	dishwasher	dishwasher
		table	beam	stainless	power	ladder	vent	vent
		tv	beam	stainless	power	bookshelf	coat rack	coat rack
		tv stand	beam	stainless	power	shelf	calendar	calendar
		vacuum cleaner	beam	stainless	power	ledge	bin	bin
			beam	stainless	power	pillar	toilet paper	projector screen
			beam	stainless	power	toilet paper	music stand	

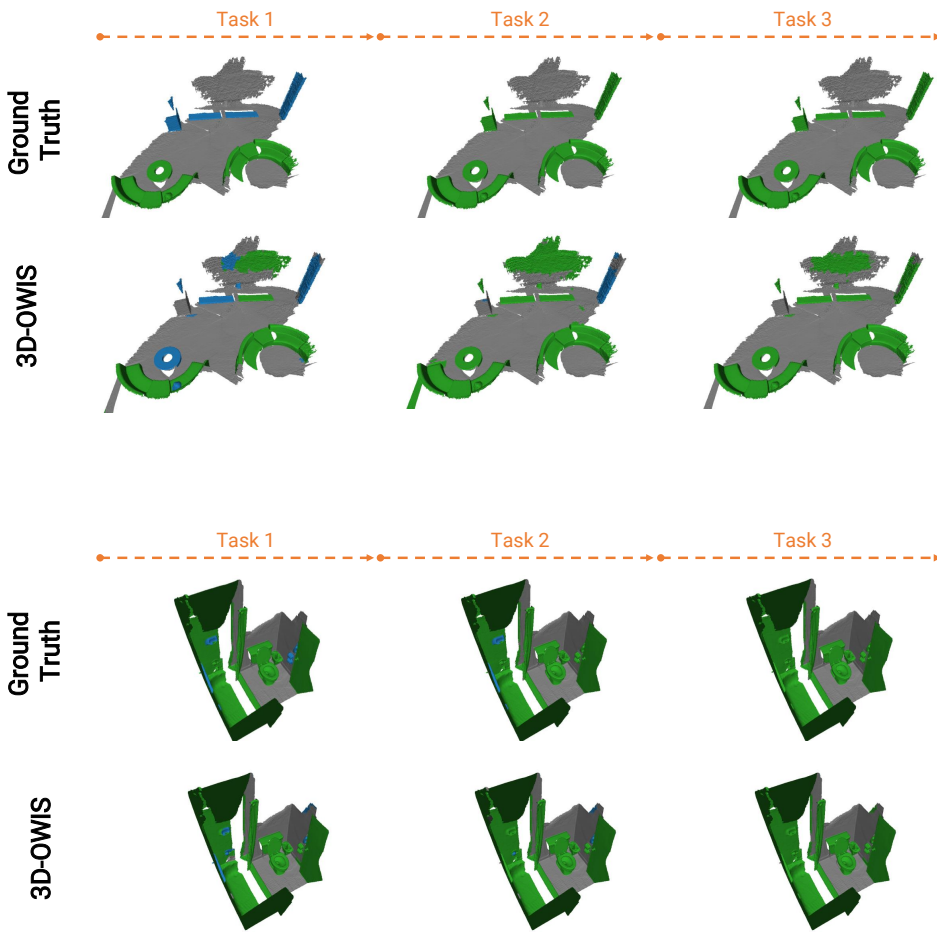


Figure 9: Alleviating catastrophic forgetting during incremental learning. The capability of **3D-OWIS** in retaining knowledge of the previously known classes after learning the new one is demonstrated across Task 2 and Task 3 for both scenes, where all objects of old known classes are still being predicted as known.

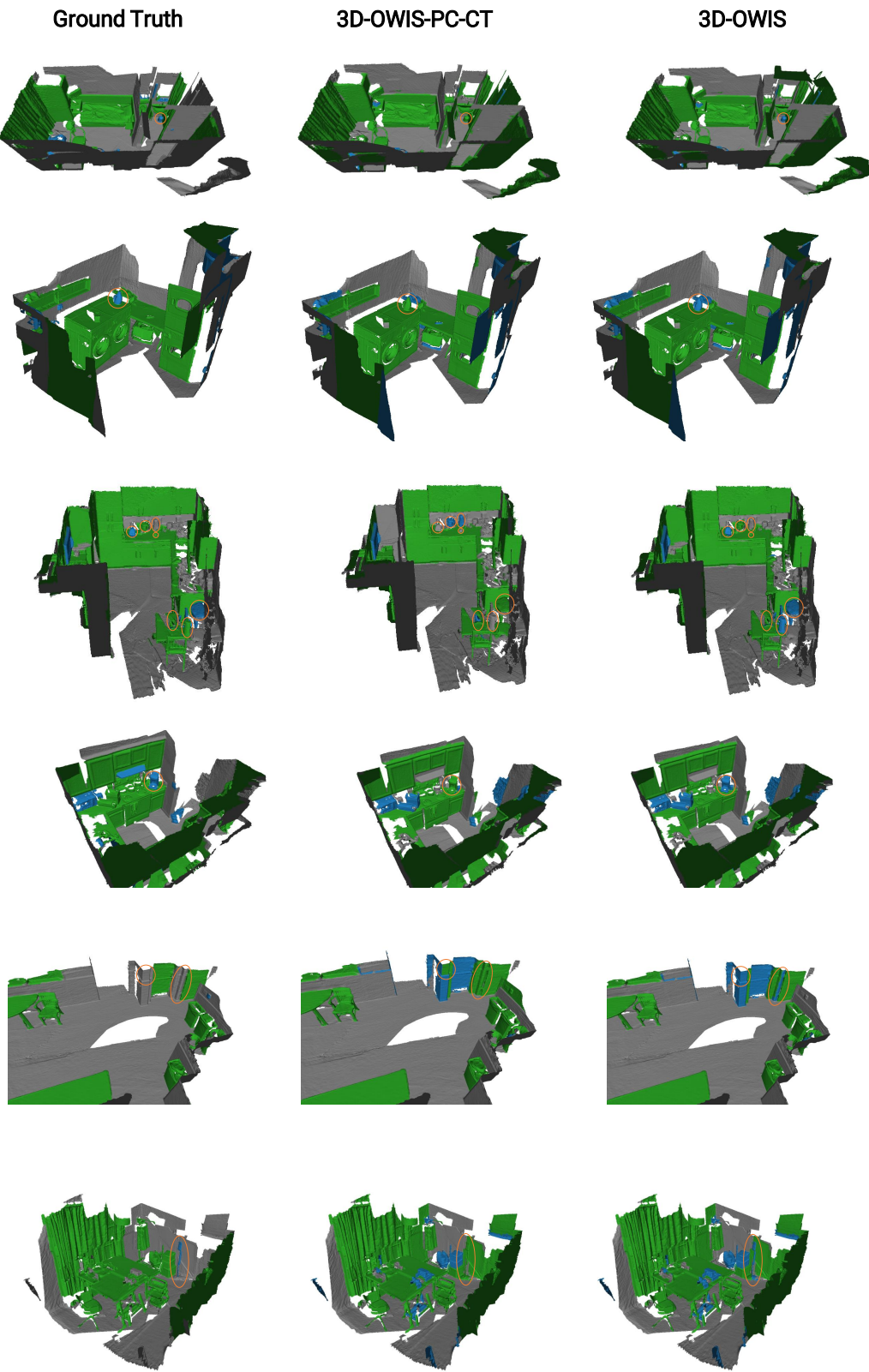


Figure 10: **Qualitative results.** The objects depicted in green represent the known classes, while the ones in blue represent the "unknown" class, and the gray objects represent the background. To emphasize the differences between 3D-OWIS and 3D-OWIS-PC-CT, we highlight them with orange circles.

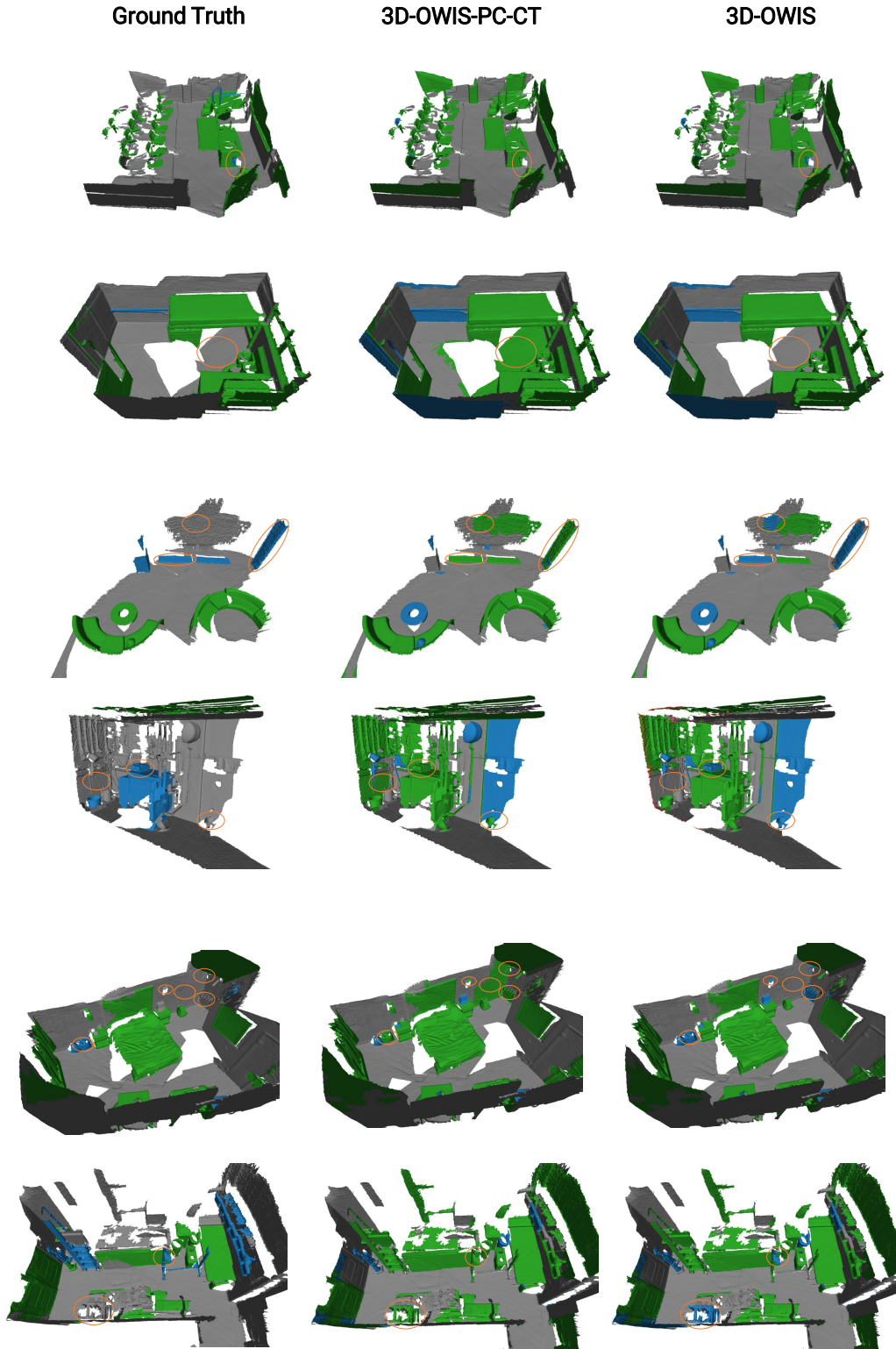


Figure 11: **Additional qualitative results** We demonstrate the better performance of our model in accurately identifying background objects (depicted in gray) as unknown (represented by the blue color), and also correcting the predictions from known class to unknown class. This capability greatly reduces the misclassification of background objects as known objects, leading to improved overall classification accuracy.

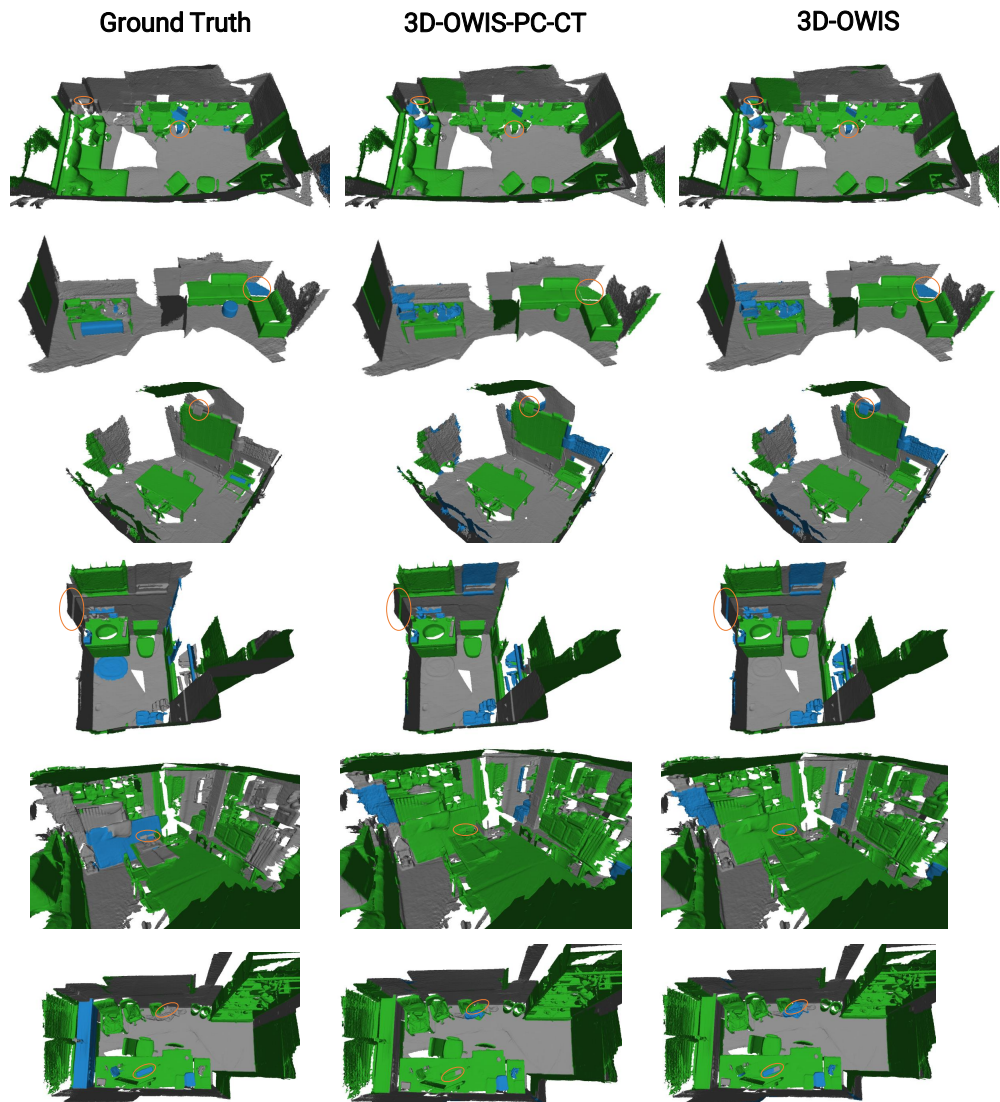


Figure 12: Additional qualitative results

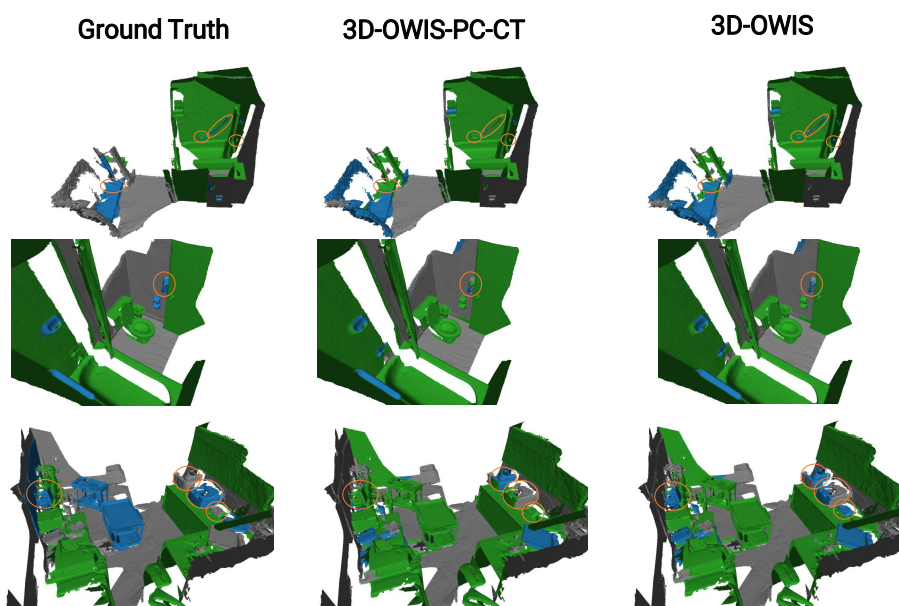


Figure 13: **Additional qualitative results**